



OPEN

## Elevated cerebral blood flow proxy with increased beta-amyloid burden in Alzheimer's disease preclinical phase evaluated by dual-phase $^{18}\text{F}$ -florbetaben positron emission tomography

Geon Ha Kim<sup>1</sup>, Bori R. Kim<sup>1,2</sup>, Hai-Jeon Yoon<sup>3,4</sup>✉ & Jee Hyang Jeong<sup>1,4</sup>✉

This study investigated the earliest change of cerebral blood flow (CBF) and its relationship with  $\beta$ -amyloid ( $\text{A}\beta$ ) burden in preclinical Alzheimer's disease (AD) employing dual-phase  $^{18}\text{F}$ -florbetaben (FBB) PET. Seventy-one cognitively normal (NC) individuals were classified as  $\text{A}\beta$  negative ( $\text{A}\beta^{-}\text{NC}$ ) or positive ( $\text{A}\beta^{+}\text{NC}$ ) based on two different cutoff values: an SUVR of  $>1.08$  and a Centiloid scale of  $>20$ . The PET scans were acquired in two phases: an early phase (0–10 min, eFBB) and a delayed phase (90–110 min, dFBB), which were averaged to generate single-frame images for each phase. Furthermore, an R1 parametric map was generated from the early phase data using a simplified reference tissue model. We conducted regional and voxel-based analyses to compare the eFBB, dFBB, and R1 images between the  $\text{A}\beta$  positive and negative groups. In addition, the correlations between the CBF proxy R1 and the dFBB SUVR were analyzed. The  $\text{A}\beta^{+}\text{NC}$  group showed significantly higher dFBB SUVR in both the global cerebral cortex and target regions compared to the  $\text{A}\beta^{-}\text{NC}$  group, while no significant differences were observed in eFBB SUVR between the two groups. Furthermore, the  $\text{A}\beta^{+}\text{NC}$  group exhibited significantly higher R1 values, a proxy for cerebral perfusion, in both the global cerebral cortex and target regions compared to the  $\text{A}\beta^{-}\text{NC}$  group. Significant positive correlations were observed between R1 and dFBB SUVR in both the global cerebral cortex and target regions, which remained significant after controlling for demographics and cognitive profiles, except for the medial temporal and occipital cortices. The findings reveal increased CBF in preclinical AD and a positive correlation between CBF and amyloid pathology. The positive correlation between R1 and amyloid burden may indicate a compensatory mechanism in the preclinical stage of Alzheimer's disease, but to elucidate this hypothesis, further longitudinal observational studies are necessary.

**Keywords**  $^{18}\text{F}$ -florbetaben, Positron emission tomography, Dual-phase, R1, Preclinical Alzheimer's disease

Alzheimer's disease (AD) stands as the most prevalent type of dementia, marked by extracellular  $\beta$ -amyloid ( $\text{A}\beta$ ) plaques and intracellular neurofibrillary tangles (NFTs) accumulation within the brain<sup>1</sup>. According to the dynamic biomarker model of AD, detecting  $\text{A}\beta$  plaque deposition, the earliest AD pathology can occur decades before the clinical symptom onset<sup>2</sup>.

Given the limited efficacy of treatments targeting  $\text{A}\beta$  protein in improving cognitive function or slowing cognitive decline in patients with symptomatic AD, and the presence of amyloid pathology before clinical manifestation, there is a growing interest in the preclinical phase as a strategic opportunity for more effective interventions<sup>3–5</sup>. However, the earliest signs of AD pathology do not necessarily correlate with clinical symptom progression, such as cognitive impairment<sup>6</sup>. Instead, alterations in regional cerebral metabolism and blood flow

<sup>1</sup>Department of Neurology, Ewha Womans University College of Medicine, Seoul, Republic of Korea. <sup>2</sup>Ewha Medical Research Institute, Ewha Womans University, Seoul, Republic of Korea. <sup>3</sup>Department of Nuclear Medicine, Ewha Womans University, College of Medicine, Seoul, Republic of Korea. <sup>4</sup>These authors contributed equally to this work: Hai-Jeon Yoon and Jee Hyang Jeong. ✉email: haijeon.yoon@ewha.ac.kr; jjeong@ewha.ac.kr

can occur during the preclinical phase of AD. Regional metabolism can be assessed using  $^{18}\text{F}$ -fluorodeoxyglucose (FDG) positron emission tomography (PET)<sup>7–9</sup>, while cerebral blood flow (CBF) can be determined via  $^{15}\text{O}$ - $\text{H}_2\text{O}$  PET<sup>10</sup> or arterial spin labeling (ASL) magnetic resonance imaging (MRI)<sup>11,12</sup>. These functional biomarkers are associated with cognitive performance and change throughout the disease, making them suitable for monitoring disease progression<sup>2,6,13</sup>.

CBF, which closely correlates with glucose metabolism, is a well-established biomarker of neuronal dysfunction in AD<sup>14</sup>. These neuronal dysfunction biomarkers are generally understood to decrease along the AD continuum as neurodegeneration progresses<sup>15,16</sup>. However, studies utilizing FDG PET have reported increased glucose metabolism in specific regions during the preclinical phase of AD, with one study reporting increases in the bilateral thalamus and bilateral superior temporal gyrus<sup>7</sup>, and another study finding increases in the posterior cingulate/precuneus, lateral parietal cortices, medial frontal cortex, and lateral prefrontal cortices<sup>9</sup>. There are also studies on CBF using ASL MRI, with one study reporting increased CBF in the hippocampus, amygdala, caudate, frontal, temporal, and insula regions during the preclinical AD phase<sup>11</sup>. Another study involving a cognitively unimpaired population reported that baseline CBF is positively associated with early amyloid- $\beta$  burden not only globally but also in the orbital-basal frontal, precuneus, and superior frontal regions in participants with a high cardiovascular risk<sup>17</sup>. Consequently, an ongoing debate has surfaced, emphasizing the necessity for further investigation.

Owing to the cost and radiation risk attributed to PET imaging, its separate use for evaluating CBF in clinical settings may be limited. However, in recent studies, alternative approaches have been explored. Specifically, using the simplified reference tissue model (SRTM) method, researchers have derived the K1 (the first-pass influx rate) ratio by dividing the K1 value of a target region by that of the reference region for the specific radiotracer, known as the delivery rate (R1), from dynamic amyloid PET scans<sup>18,19</sup>. This R1 value, indicative of relative perfusion, has shown a strong correlation with CBF measured using the gold standard method of  $^{15}\text{O}$ - $\text{H}_2\text{O}$  PET<sup>18</sup>, or a strong correlation with metabolism measured using  $^{18}\text{F}$ -FDG PET<sup>19</sup>, suggesting its potential as a biomarker for assessing neuronal dysfunction. Furthermore, our previous research has revealed that the delivery rate R1, derived from the early time point of dynamic amyloid PET scans, reliably indicates cerebral perfusion and neuronal dysfunction<sup>20</sup>. By adding an early phase dynamic acquisition to the standard amyloid PET protocol, it is possible to simultaneously obtain information on both amyloid burden and CBF. The utility of this dual-phase PET protocol is currently being investigated through the ongoing trial<sup>21</sup>.

Although cross-sectional studies on R1 have been conducted, there is a lack of research investigating CBF changes in preclinical AD using amyloid PET-derived R1. Therefore, this study aims to investigate the earliest alteration in CBF in cognitively normal individuals demonstrating A $\beta$  positivity, indicating preclinical AD, by using a dual-phase dynamic PET protocol that is easily applicable in clinical settings. We utilized CBF proxies obtained from early-phase  $^{18}\text{F}$ -florbetaben (FBB) PET scans to compare CBF between A $\beta$ -negative cognitively normal (A $\beta$ <sup>-</sup>NC) and A $\beta$ -positive cognitively normal (A $\beta$ <sup>+</sup>NC) participants. Additionally, we explored the direct correlation between the CBF proxy R1 derived from early-phase FBB PET and A $\beta$  deposition quantified from delayed-phase FBB PET scans, not only at the global level but also at the regional level.

## Results

### Demographics and cognitive profiles

Of the 71 cognitively normal participants, 40 were classified as belonging to the A $\beta$ <sup>-</sup>NC group, and 31 were classified as belonging to the A $\beta$ <sup>+</sup>NC group by the SUVR cutoff. When using the Centiloid cutoff, 47 participants were classified as belonging to the A $\beta$ <sup>-</sup>NC group, and 24 were classified as belonging to the A $\beta$ <sup>+</sup>NC group.

No significant differences were observed in the demographics and cognitive profiles between the two groups based on A $\beta$  positivity determined by the SUVR cutoff, with the exception for years of education (Table 1). The results based on A $\beta$  positivity determined by the Centiloid cutoff showed no significant differences in the demographics and cognitive profiles between the two groups, with the exception of the proportion of females (Supplemental Table 1).

### VOI-based and voxel-based comparison of dFBB SUVR between the A $\beta$ <sup>-</sup>NC and A $\beta$ <sup>+</sup>NC groups

The global dFBB SUVR was significantly higher in the A $\beta$ <sup>+</sup>NC group than in the A $\beta$ <sup>-</sup>NC group based on A $\beta$  positivity determined by the SUVR cutoff ( $1.03 \pm 0.03$  vs.  $1.18 \pm 0.12$ ,  $p < 0.001$ ; Fig. 1A). All target regional SUVRs were also significantly higher in the A $\beta$ <sup>+</sup>NC group than in the A $\beta$ <sup>-</sup>NC group (frontal cortex:  $1.03 \pm 0.04$  vs.  $1.20 \pm 0.15$ ,  $p < 0.001$ ; PCC/PC:  $1.10 \pm 0.07$  vs.  $1.29 \pm 0.22$ ,  $p < 0.001$ ; lateral parietal cortex:  $0.94 \pm 0.05$  vs.  $1.14 \pm 0.15$ ,  $p < 0.001$ ; lateral temporal cortex:  $0.96 \pm 0.03$  vs.  $1.10 \pm 0.12$ ,  $p < 0.001$ ; medial temporal cortex:  $1.04 \pm 0.05$  vs.  $1.09 \pm 0.06$ ,  $p = 0.003$ ; occipital cortex:  $1.06 \pm 0.06$  vs.  $1.20 \pm 0.12$ ,  $p < 0.001$ ; Fig. 2A–F). The results based on A $\beta$  positivity determined by the Centiloid cutoff are presented in Supplemental Figs. 1A and 2A–F).

The voxel-wise analysis revealed significant increases in amyloid burden throughout the neocortex in the A $\beta$ <sup>+</sup>NC compared to the A $\beta$ <sup>-</sup>NC group, based on A $\beta$  positivity determined by both the SUVR and the Centiloid cutoff (FDR-corrected  $p < 0.05$ , Fig. 3A–B).

### VOI-based and voxel-based comparison of eFBB SUVR between the A $\beta$ <sup>-</sup>NC and A $\beta$ <sup>+</sup>NC groups

The global eFBB SUVR did not differ significantly between the groups based on A $\beta$  positivity determined by the SUVR cutoff ( $0.92 \pm 0.04$  vs.  $0.93 \pm 0.03$ ,  $p = 0.170$ ; Fig. 1B). In addition, none of the target regions showed significant differences in eFBB SUVR between the groups (frontal cortex:  $0.93 \pm 0.04$  vs.  $0.94 \pm 0.03$ ,  $p = 0.280$ ; PCC/PC:  $0.92 \pm 0.05$  vs.  $0.94 \pm 0.05$ ,  $p = 0.178$ ; lateral parietal cortex:  $0.91 \pm 0.05$  vs.  $0.92 \pm 0.04$ ,  $p = 0.124$ ; lateral temporal cortex:  $0.89 \pm 0.04$  vs.  $0.90 \pm 0.04$ ,  $p = 0.192$ ; medial temporal cortex:  $0.71 \pm 0.03$  vs.  $0.71 \pm 0.04$ ,  $p = 0.841$ ;

	Total (n = 71)	A $\beta$ <sup>-</sup> NC (n = 40)	A $\beta$ <sup>+</sup> NC (n = 31)	p-value
Demographics				
Age, years	73.24 ± 5.57	72.78 ± 5.43	73.84 ± 5.79	0.433
Female, %	78.87%	86.64%	75.00%	> 0.99
Education, years	9.82 ± 4.17	10.78 ± 4.16	8.58 ± 3.91	0.025*
APOE4 carrier†	18.18%	13.16%	25.00%	0.362
Cognitive profiles				
MMSE score	28.38 ± 1.44	28.45 ± 1.4	28.29 ± 1.51	0.649
Global CDR	0.31 ± 0.24	0.35 ± 0.23	0.26 ± 0.25	0.121
Attention				
Digit span Forward	0.26 ± 0.96	0.32 ± 0.94	0.18 ± 0.99	0.549
Digit span Backward	0.3 ± 0.98	0.39 ± 1.16	0.19 ± 0.68	0.350
Language				
Naming K-BNT	0.2 ± 0.91	0.21 ± 0.74	0.18 ± 1.1	0.881
Visuospatial				
RCFT copy	0.06 ± 0.9	0.17 ± 0.7	-0.08 ± 1.11	0.273
Memory				
SVLT Delayed recall	0.59 ± 0.98	0.57 ± 1	0.61 ± 0.96	0.873
RCFT delayed recall	0.37 ± 1.01	0.32 ± 0.97	0.45 ± 1.07	0.596
Frontal Executive function				
COWAT phonemic	0.78 ± 1.28	0.8 ± 1.4	0.74 ± 1.12	0.849
StroopTest Color reading correct	0.51 ± 0.9	0.61 ± 0.86	0.39 ± 0.95	0.321

**Table 1.** Demographics and cognitive profiles (A $\beta$  positivity determined by the SUVR cutoff). Values are expressed as mean with standard deviation. *p*-values were calculated using the Two sample *t*-test. \**p*-values indicate significance at the 0.05 level. †APOE4 genotyping was missed in two participants in the A $\beta$ <sup>-</sup>NC group and four participants in the A $\beta$ <sup>+</sup>NC group. A $\beta$ <sup>-</sup>NC, A $\beta$ -negative cognitively normal; A $\beta$ <sup>+</sup>NC, A $\beta$ -positive cognitively normal; APOE, apolipoprotein E; MMSE, Mini-Mental State Examination; CDR, Clinical Dementia Rating; K-BNT, Korean version of the Boston Naming Test; RCFT, Rey–Osterrieth Complex Figure Test; SVLT, Seoul Verbal Learning Test; COWAT, Controlled Oral Word Association Test.

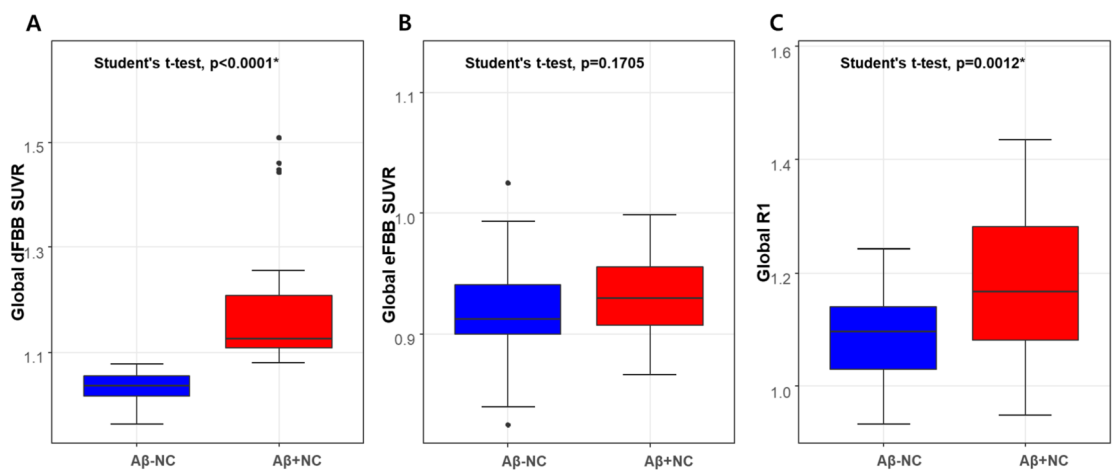


**Figure 1.** Comparing the global dFBB SUVR, eFBB SUVR, and R1 between the A $\beta$ <sup>-</sup>NC and A $\beta$ <sup>+</sup>NC groups (A $\beta$  positivity determined by the SUVR cutoff). The global dFBB SUVR (A) showed significant A $\beta$  depositions in the A $\beta$ <sup>+</sup>NC group compared to the A $\beta$ <sup>-</sup>NC group. The global eFBB SUVR (B) showed no significant difference between the groups. The global R1 (C) showed a significant perfusion increase in the A $\beta$ <sup>+</sup>NC group compared to the A $\beta$ <sup>-</sup>NC group.

occipital cortex:  $0.95 \pm 0.05$  vs.  $0.96 \pm 0.03$ , *p* = 0.512; Fig. 4A–F). The results based on A $\beta$  positivity determined by the Centiloid cutoff are presented Supplemental Figs. 1B and 3A–F).

Figure 5 shows the analysis results at the voxel level between the A $\beta$ <sup>-</sup>NC and A $\beta$ <sup>+</sup>NC group. The eFBB perfusion was not significantly different between the A $\beta$ <sup>+</sup>NC compared to the A $\beta$ <sup>-</sup>NC group (uncorrected *p* < 0.001).

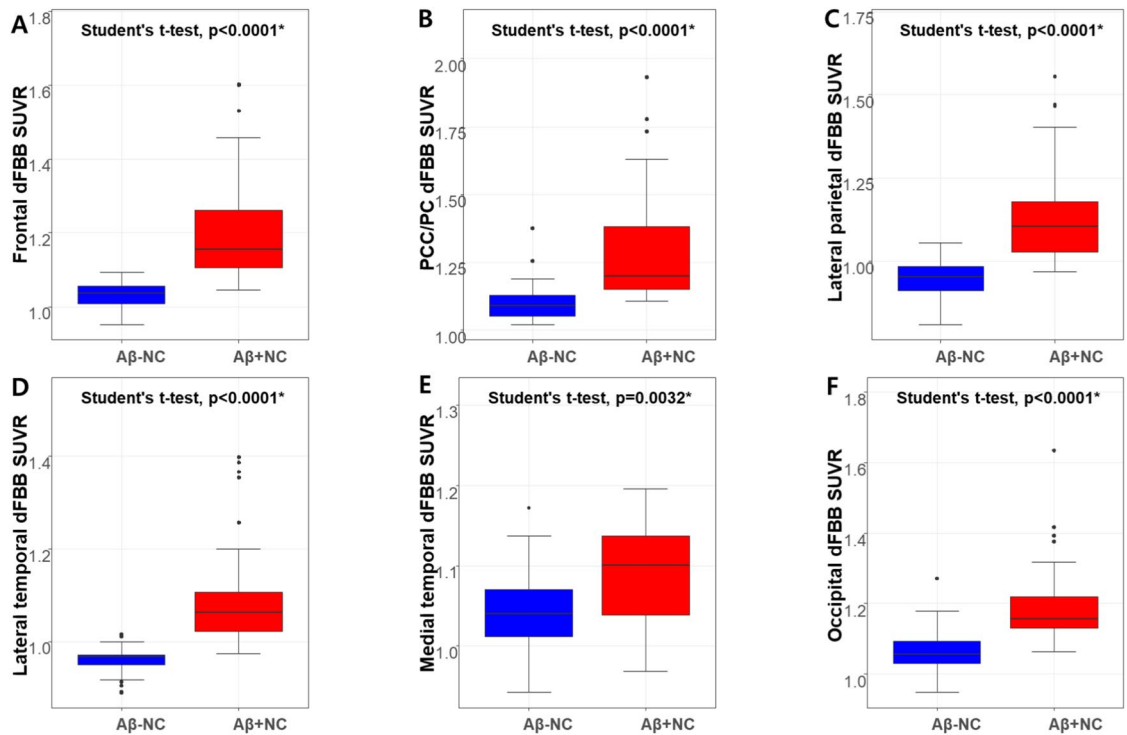


**Figure 2.** Comparing the target regional dFBB SUVR between the Aβ<sup>-</sup>NC and Aβ<sup>+</sup>NC groups (Aβ positivity determined by the SUVR cutoff). Compared with the Aβ<sup>-</sup>NC group, the target regional dFBB SUVR showed significant Aβ depositions in the Aβ<sup>+</sup>NC group in (A) frontal, (B) posterior cingulate and precuneus, (C) lateral parietal, (D) lateral temporal, (E) medial temporal, and (F) occipital cortices.

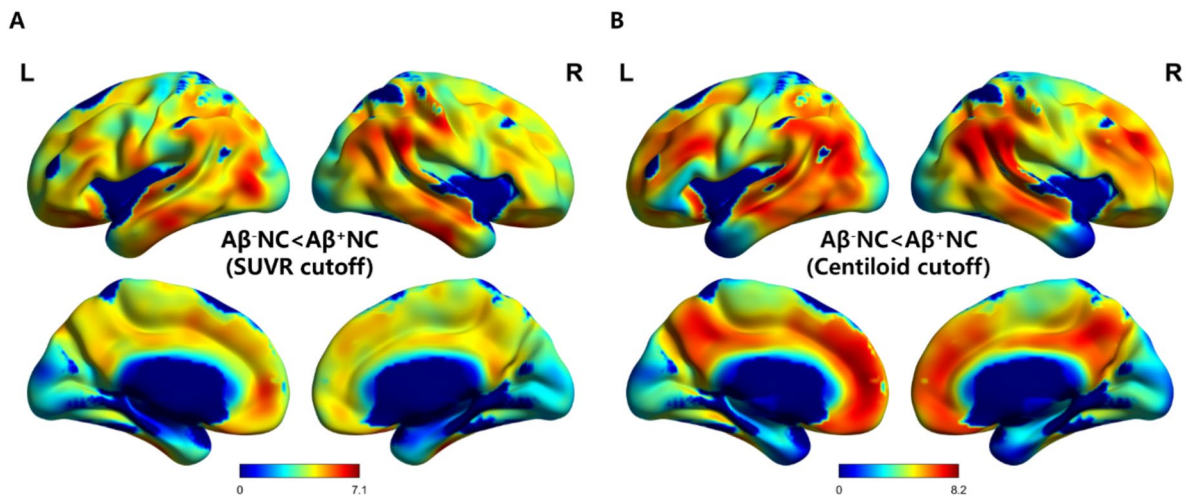


**Figure 3.** Statistical parametric maps from a voxel-based comparison of dFBB SUVR between the Aβ<sup>-</sup>NC and Aβ<sup>+</sup>NC groups. Statistical parametric maps reveal typical AD target regions showing Aβ accumulation patterns in the Aβ<sup>+</sup>NC group compared to the Aβ<sup>-</sup>NC group. (A) shows results using Aβ positivity determined by the SUVR cutoff, while (B) shows results using Aβ positivity determined by the Centiloid cutoff (FDR-corrected  $p < 0.05$ ,  $t > 1.8$ , cluster extent of more than 100 voxels).

### VOI-based and voxel-based comparison of R1 between the Aβ<sup>-</sup>NC and Aβ<sup>+</sup>NC groups

The global R1 was significantly higher in the Aβ<sup>+</sup>NC group than in the Aβ<sup>-</sup>NC group based on Aβ positivity determined by the SUVR cutoff ( $1.09 \pm 0.08$  vs.  $1.18 \pm 0.14$ ,  $p = 0.001$ ; Fig. 1C). Additionally, all target regional R1 values were significantly higher in the Aβ<sup>+</sup>NC group than in the Aβ<sup>-</sup>NC group (frontal cortex:  $1.18 \pm 0.08$  vs.  $1.28 \pm 0.15$ ,  $p = 0.002$ ; PCC/PC:  $1.21 \pm 0.09$  vs.  $1.31 \pm 0.15$ ,  $p = 0.002$ ; lateral parietal cortex:  $1.11 \pm 0.09$  vs.  $1.20 \pm 0.14$ ,  $p = 0.002$ ; lateral temporal cortex:  $1.07 \pm 0.08$  vs.  $1.17 \pm 0.14$ ,  $p = 0.001$ ; medial temporal cortex:  $0.85 \pm 0.07$  vs.  $0.92 \pm 0.11$ ,  $p = 0.004$ ; occipital cortex:  $1.14 \pm 0.10$  vs.  $1.24 \pm 0.15$ ,  $p = 0.002$ ; Fig. 6A–F). The results based on Aβ positivity determined by the Centiloid cutoff are presented Supplemental Figs. 1C and 4A–F).

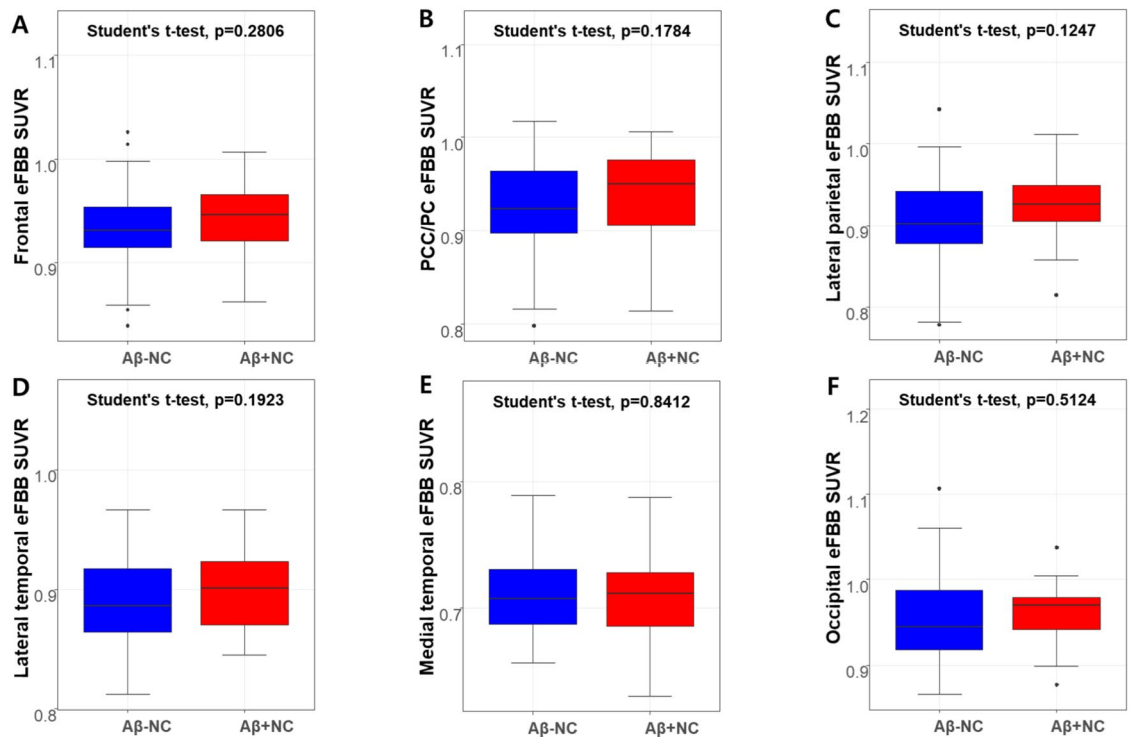


**Figure 4.** Comparing the target regional eFBB SUVR between the  $A\beta^{-}NC$  and  $A\beta^{+}NC$  groups ( $A\beta$  positivity determined by the SUVR cutoff). The comparison between the  $A\beta^{-}NC$  and  $A\beta^{+}NC$  groups did not show significant differences in the target regional eFBB SUVR in any of (A) frontal, (B) posterior cingulate and precuneus, (C) lateral parietal, (D) lateral temporal, (E) medial temporal, and (F) occipital cortices.

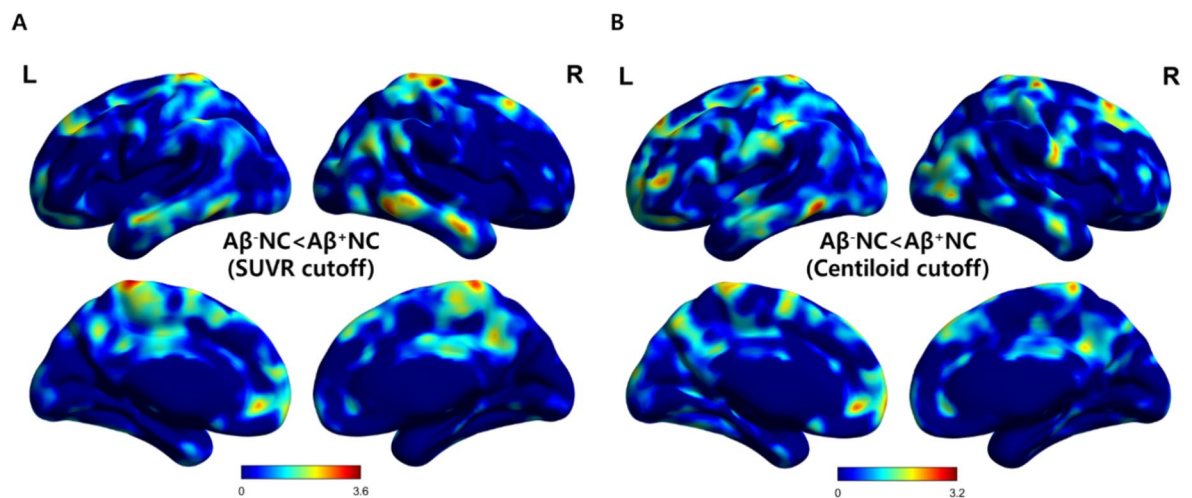


**Figure 5.** Statistical parametric maps from a voxel-based comparison of eFBB SUVR between the  $A\beta^{-}NC$  and  $A\beta^{+}NC$  groups. The eFBB perfusion in the cortical regions was not significantly different between the  $A\beta^{-}NC$  and  $A\beta^{+}NC$  groups. (A) shows results using  $A\beta$  positivity determined by the SUVR cutoff, while (B) shows results using  $A\beta$  positivity determined by the Centiloid cutoff (uncorrected  $p < 0.001$ ,  $t > 3.2$ , cluster extent of more than 100 voxels).

Figure 7 shows the analysis findings at the voxel level between the  $A\beta^{-}NC$  and  $A\beta^{+}NC$  groups. The voxel-wise analysis revealed significant increases in R1 perfusion across the neocortex in the  $A\beta^{+}NC$  group compared to those in the  $A\beta^{-}NC$  group, based on  $A\beta$  positivity determined by both the SUVR and the Centiloid cutoff (FDR-corrected  $p < 0.05$ ).

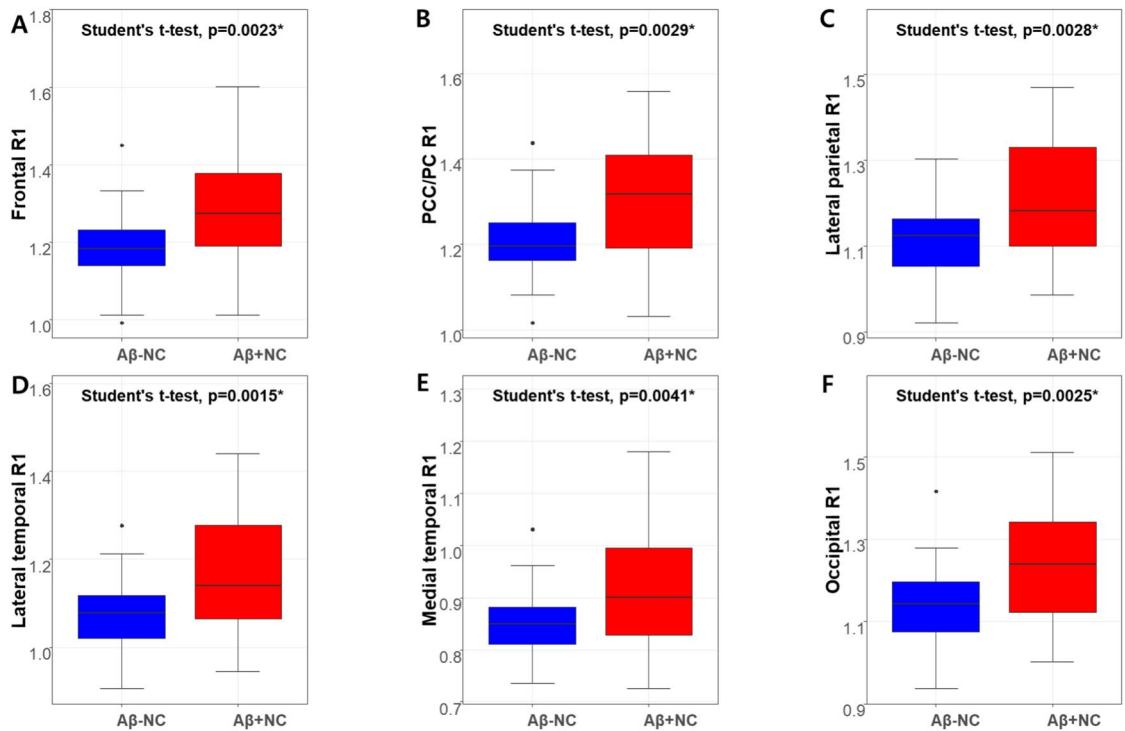


**Figure 6.** Comparing the target regional R1 between the  $A\beta^{-}NC$  and  $A\beta^{+}NC$  groups ( $A\beta$  positivity determined by the SUVR cutoff). Compared with the  $A\beta^{-}NC$  group, the target regional R1 showed significant increase of perfusion in the  $A\beta^{+}NC$  group in (A) frontal, (B) posterior cingulate and precuneus, (C) lateral parietal, (D) lateral temporal, (E) medial temporal, and (F) occipital cortices.

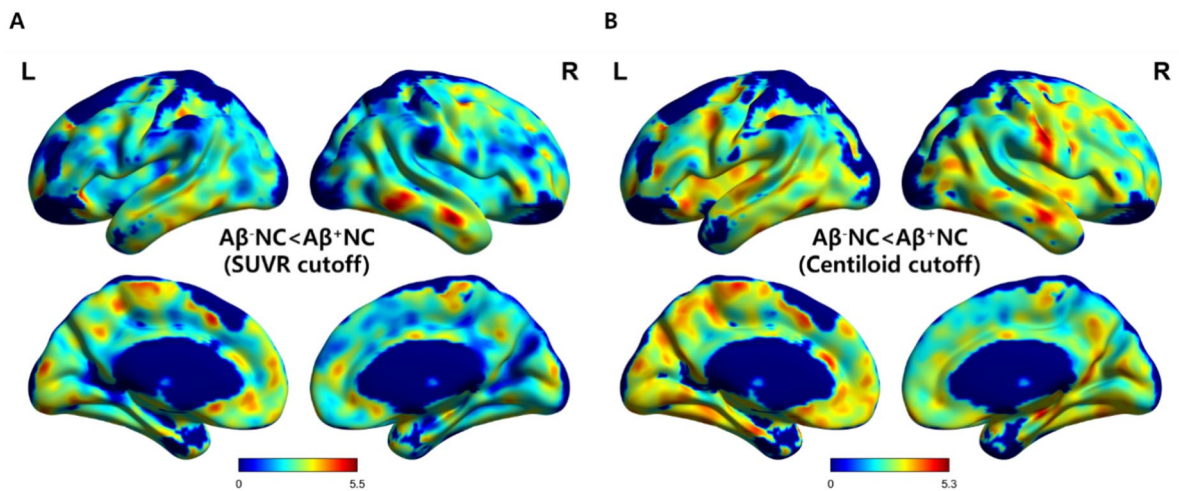


**Figure 7.** Statistical parametric maps from a voxel-based comparison of R1 between the  $A\beta^{-}NC$  and  $A\beta^{+}NC$  groups. Statistical parametric maps reveal hyper-perfusion patterns in the  $A\beta^{+}NC$  compared with the  $A\beta^{-}NC$  group. (A) shows results using  $A\beta$  positivity determined by the SUVR cutoff, while (B) shows results using  $A\beta$  positivity determined by the Centiloid cutoff (FDR-corrected  $p < 0.05$ ,  $t > 1.7$ , cluster extent of more than 100 voxels).

### Correlations between CBF proxy R1 and amyloid burden

A significant positive correlation was observed between global R1 and dFBB SUVR ( $r = 0.464$ ,  $p < 0.001$ , Fig. 8A). Of the target regions, significant positive correlations between R1 and SUVR were evident in the frontal ( $r = 0.519$ ,  $p < 0.001$ , Fig. 8B), PCC/PC ( $r = 0.401$ ,  $p < 0.001$ , Fig. 8C), lateral parietal ( $r = 0.351$ ,  $p = 0.002$ , Fig. 8D), lateral temporal ( $r = 0.414$ ,  $p < 0.001$ , Fig. 8E), and medial temporal ( $r = 0.267$ ,  $p = 0.024$ , Fig. 8F) cortices. However, the occipital cortex ( $r = 0.231$ ,  $p = 0.052$ , Fig. 8G) did not show a significant correlation. After controlling for age, gender, years of education, and the CDR score, significant positive correlations were observed between R1 and dFBB SUVR in the global ( $r = 0.462$ ,  $p < 0.001$ ) as well as in the target regions, except for the medial temporal

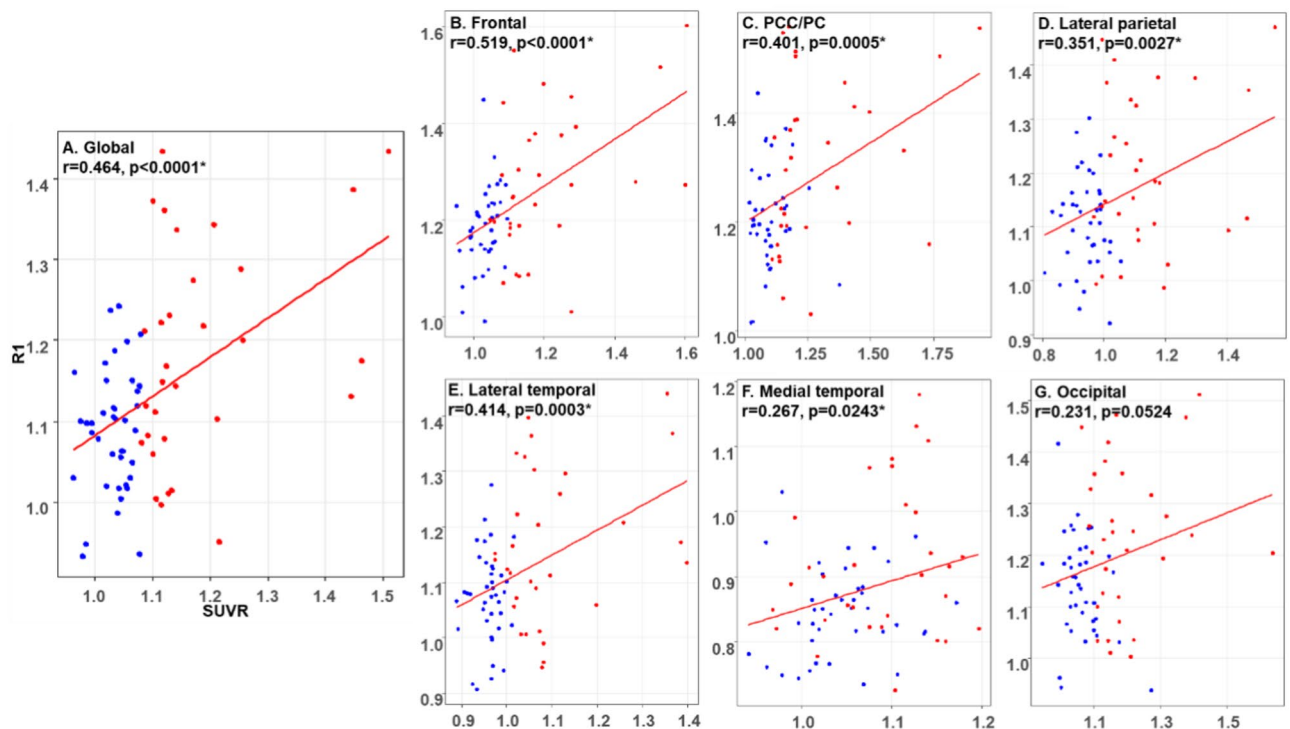


**Figure 8.** Scatter plots between the cerebral perfusion proxy R1 with amyloid burden dFBB SUVR at both the global (A) and regional (B–G) levels. At the global level (A), a significant positive correlation between R1 and dFBB SUVR, suggesting that higher amyloid burden is associated with increased cerebral perfusion. Similar significant positive correlations are observed at the regional level (B–F). The occipital region (G) showed a trend towards significance. Blue dots indicate  $A\beta^{-}NC$ , while red dots indicate  $A\beta^{+}NC$ .

cortex (frontal cortex:  $r = 0.518$ ,  $p < 0.001$ ; PCC/PC:  $r = 0.404$ ,  $p < 0.001$ ; lateral parietal:  $r = 0.368$ ,  $p = 0.002$ ; lateral temporal:  $r = 0.407$ ,  $p < 0.001$ ; medial temporal:  $r = 0.218$ ,  $p = 0.076$ ; occipital:  $r = 0.249$ ,  $p = 0.042$ ).

### Relationship of cognitive profiles with CBF proxy R1 and amyloid burden

When analyzing the correlation between global R1 and individual cognitive profiles, no significant correlations were observed in any cognitive domain, including attention, language, visuospatial, memory, and frontal executive function. Similarly, no statistically significant correlations were found between global dFBB SUVR and individual cognitive profiles (Table 2).

### Comparison of R1 across low, intermediate, and high amyloid burden groups

Based on the Centiloid scale cutoffs of 20 and 40, participants were classified into three groups: low (Centiloid  $< 20$ ,  $n = 47$ ), intermediate (Centiloid  $20\text{--}40$ ,  $n = 15$ ), and high (Centiloid  $> 40$ ,  $n = 9$ ) amyloid burden. The results showed a significant difference among groups and a gradual increase in global R1 values with increasing amyloid burden (low:  $1.09 \pm 0.08$  vs. intermediate:  $1.19 \pm 0.13$  vs. high:  $1.22 \pm 0.15$ ,  $p = 0.0109$ ; Supplemental Fig. 5). Post-hoc analyses revealed a significant global R1 increase in the intermediate and high groups compared to the low group ( $p = 0.0122$  and  $p = 0.0015$ , respectively), but no statistically significant difference between the intermediate and high groups ( $p = 0.3964$ ).

The significant difference among groups and the gradual increase in R1 values with increasing amyloid burden were also observed in the frontal (low:  $1.19 \pm 0.09$  vs. intermediate:  $1.28 \pm 0.13$  vs. high:  $1.33 \pm 0.18$ ,  $p = 0.0158$ ; Supplemental Fig. 6A), PCC/PC (low:  $1.22 \pm 0.1$  vs. intermediate:  $1.32 \pm 0.15$  vs. high:  $1.32 \pm 0.17$ ,  $p = 0.0312$ ; Supplemental Fig. 6B), lateral parietal (low:  $1.11 \pm 0.09$  vs. intermediate:  $1.21 \pm 0.14$  vs. high:  $1.23 \pm 0.17$ ,  $p = 0.0221$ ; Supplemental Fig. 6C), lateral temporal (low:  $1.08 \pm 0.09$  vs. intermediate:  $1.16 \pm 0.12$  vs. high:  $1.21 \pm 0.16$ ,  $p = 0.0134$ ; Supplemental Fig. 6D), medial temporal (low:  $0.85 \pm 0.08$  vs. intermediate:  $0.92 \pm 0.11$  vs. high:  $0.96 \pm 0.12$ ,  $p = 0.0177$ ; Supplemental Fig. 6E), and occipital (low:  $1.14 \pm 0.09$  vs. intermediate:  $1.25 \pm 0.16$  vs. high:  $1.29 \pm 0.15$ ,  $p = 0.0117$ ; Supplemental Fig. 6F) cortices.

### Discussion

In this study, we investigated the alteration in CBF in cognitively normal individuals demonstrating  $A\beta$  positivity, indicating preclinical AD, by using a dual-phase dynamic PET protocol. The study participants were divided into  $A\beta^{-}NC$  and  $A\beta^{+}NC$  groups based on two different cutoffs: SUVR and Centiloid. The results showed significantly higher global and regional R1 values in the  $A\beta^{+}NC$  group compared to the  $A\beta^{-}NC$  group, indicating increased relative perfusion, while no significant differences were observed in eFBB SUVR between the two

	Global R1		Global dFBB SUVR	
	rho coefficient	p-value	rho coefficient	p-value
Attention				
Digit span Forward	-0.153	0.210	0.050	0.683
Digit span Backward	0.013	0.915	-0.027	0.823
Language				
Naming K-BNT	0.092	0.453	0.317	0.752
Visuospatial				
Rey CFT copy	-0.033	0.789	-0.113	0.356
Memory				
SVLT delayed recall	-0.023	0.851	-0.138	0.260
RCFT delayed recall	-0.135	0.271	-0.050	0.680
Frontal Executive function				
COWAT phonemic	-0.119	0.330	-0.062	0.615
StroopTest Color reading correct	-0.049	0.687	-0.201	0.099

**Table 2.** Relationships of cognitive profiles with R1 and dFBB SUVR. \**p*-values indicate significance at the 0.05 level. dFBB, delayed phase florbetaben; SUVR, standardized uptake value ratio; K-BNT, Korean version of the Boston Naming Test; RCFT, Rey–Osterrieth Complex Figure Test; SVLT, Seoul Verbal Learning Test; COWAT, Controlled Oral Word Association Test.

groups. Furthermore, significant positive correlations were found between R1 and dFBB SUVR globally and in most target regions, even after controlling for demographics and cognitive profiles. These findings suggest that increased amyloid burden is associated with higher relative perfusion in cognitively normal individuals.

According to the dynamic biomarker model of AD, it is widely accepted that metabolism, reflecting neuronal dysfunction, decreases throughout the AD continuum. Consequently, a corresponding decrease in close coupling CBF was observed<sup>2</sup>. Furthermore, substantial preclinical and clinical evidence supports the proposal of neurovascular pathways to neurodegeneration, which aligns with this decrease in CBF<sup>16</sup>. These pathways primarily revolve around vascular dysfunction, encompassing the disruption of the blood–brain barrier, hypoperfusion-hypoxia, and metabolic dysfunction in endothelial cells. Additionally, A $\beta$  is known to narrow cerebral arteries<sup>22</sup>. In a murine AD model, dysfunction of the endothelium-dependent regulation of neocortical microcirculation occurs before A $\beta$  accumulation<sup>23,24</sup>. Additionally, patients with AD and mouse models demonstrating increased levels of transcription factors controlling the differentiation of vascular smooth muscle cells have shown the development of a hypercontractile arterial phenotype. This condition leads to brain hypoperfusion, diminished functional hyperemia, and cerebral amyloid angiopathy<sup>25,26</sup>. The hypoperfusion resulting from this vascular dysfunction is widely acknowledged, uncontroversially, during the stages of MCI and AD, both of which are characterized by cognitive impairment<sup>27,28</sup>.

However, studies have reported an increase in metabolism and CBF in specific regions during the preclinical stage. Johnson et al. investigated the link between A $\beta$  and neural function in normal adults at risk of AD using FDG PET<sup>7</sup>. They found that A $\beta$ <sup>+</sup> participants demonstrated elevated glucose metabolisms in the bilateral thalamus and bilateral superior temporal gyrus compared to those in the A $\beta$ <sup>-</sup> group. Oh et al. evaluated the relationship between topographical patterns of A $\beta$  deposition and glucose metabolism in cognitively normal elderly individuals<sup>9</sup>. They found that those with higher A $\beta$  deposition showed relative hypermetabolism in the brain regions correlated with the network in the default mode, such as the posterior cingulate/precuneus, lateral parietal cortices, medial frontal cortex, and lateral prefrontal cortices. Fazlollahi et al. investigated the relationship between CBF, measured by ASL MRI, and A $\beta$  burden in a study involving cognitively normal participants ( $\geq 65$  years)<sup>11</sup>. They observed a positive correlation between CBF and A $\beta$  burden in various brain regions, including the hippocampus, amygdala, caudate, frontal, temporal, and insula cortices.

Such observations suggest an early compensatory mechanism. The increase in CBF indicates heightened brain function. During the preclinical AD phase, marked by preserved cognitive function, increases in regional CBF suggest cellular and vascular compensatory responses to A $\beta$  pathological buildup<sup>29</sup>. Other studies involving nondemented elderly individuals at risk for AD have also revealed marked increases in CBF in the hippocampus and medial temporal lobe. These increases have been interpreted as compensatory mechanisms providing additional glucose and oxygen to support neuronal activity<sup>30,31</sup>. Additionally, multiple functional MRI studies have revealed elevated neural activities during cognitive tasks in cognitively normal individuals with A $\beta$ <sup>+</sup> compared to both young individuals and cognitively normal older individuals with A $\beta$ <sup>-</sup><sup>32,33</sup>. Moreover, a recent study by Padrela et al. in a cognitively unimpaired population reported that baseline CBF is positively associated with early A $\beta$  burden not only globally but also in the orbital-basal frontal, precuneus, and superior frontal regions in participants with a high Framingham Risk Score, which defines the cardiovascular risk profile<sup>17</sup>. They interpreted this as a vascular compensatory response in the early stages of AD pathology. In this study, we observed substantial associations between CBF proxy R1 and A $\beta$  burden in most neocortical regions. The positive correlation between R1 and A $\beta$  suggests a relationship between relative perfusion and amyloid pathology in the preclinical stage of Alzheimer's disease. However, the current analysis does not allow for inferring directionality or causal



relationships between these factors. Longitudinal studies monitoring CBF and metabolism in cognitively normal individuals with  $A\beta^+$  have consistently shown declines over time, suggesting a potential deterioration in the neuronal dysfunction biomarker along the AD progression pathway<sup>8,10,34</sup>. On the other hand, a recent study by Padrela et al. found that in a cognitively unimpaired population, participants with positive amyloid PET, especially those who remained persistently positive, showed a significant increase in CBF in the precuneus region over a 4-year follow-up period<sup>17</sup>. The discrepancy between these longitudinal results may arise from differences in the specific sub-stages of the preclinical phase among the participants included in the studies or from variations in the follow-up duration. To further elucidate the complex interplay between CBF and amyloid accumulation in the asymptomatic stage, longitudinal observational studies monitoring  $A\beta$  and CBF changes in cognitively normal individuals with  $A\beta^-$  but at high risk of AD, based on factors such as genetic risk (e.g., APOE  $\epsilon 4$  allele), family history of AD, or subjective cognitive decline, are needed.

The ASL MRI technique is widely utilized for CBF measurement owing to its radiation-free nature and patient convenience.  $^{15}\text{O}$ - $\text{H}_2\text{O}$  PET is deemed the gold standard for CBF quantification; however, it is less preferred than MRI owing to its radiation exposure. Additionally, the extremely short half-life of the  $^{15}\text{O}$  radioisotope restricts its widespread utilization, as it necessitates specialized facilities with cyclotron production capabilities. Therefore, there have been efforts to explore alternative modalities. According to Otttoy et al., both early-phase  $^{18}\text{F}$ -florbetapir (eAV45) SUVR and R1 values obtained from full dynamic scans showed strong correlations with the gold standard CBF<sup>18</sup>. However, they reported that eAV45 SUVR tended to underestimate CBF reduction, showed weaker correlations with cognition profiles, and exhibited lower discriminative capacity in the hippocampus, precuneus, and posterior cingulate compared to R1. They proposed that R1 serves as a more reliable measure of CBF than the eAV45. However, the lengthy process of dynamic scanning limits its routine application. In our previous research, we derived R1 values from the initial 10 min of dynamic scans. We found it to be a robust indicator of cerebral perfusion and neuronal dysfunction<sup>20</sup>. We previously observed R1 reductions in the precuneus region in MCI compared to controls and widespread R1 reductions in frontal, temporal, and parietal cortical regions in AD compared to MCI. Furthermore, in our present investigation targeting preclinical AD, we observed increased R1 levels compared to individuals with  $A\beta^-$ NC.

Through the application of our dual-phase FBB PET protocol, we can simultaneously acquire information on amyloid burden and neurodegeneration, which correspond to the “A” and “N” components of the ATN biomarker framework, respectively. This approach facilitates a direct comparison between amyloid burden and neurodegeneration within the same patient and at the same time point<sup>35</sup>. The potential of such dual-phase protocols is further supported by ongoing large-scale studies like the Amyloid Imaging to Prevent Alzheimer’s Disease (AMYPAD) project<sup>21</sup>. This project is implementing a dynamic dual-time window acquisition protocol to enhance quantitative amyloid PET imaging in a large-scale population in the early stages of AD, aiming to provide more comprehensive insights into disease progression and improve diagnostic accuracy. Not only this project, but also previous studies have suggested 0–30 min as an optimal early time point for a dual-time window protocol to accurately estimate binding potential ( $\text{BP}_{\text{ND}}$ ,  $A\beta$  load)<sup>36,37</sup>. However, Heeman et al. also found only a small error in SRTM-derived R1 for the 0–10 and 90–110 min protocol, which would be negligible for practical applications<sup>37</sup>. This suggests that obtaining the early time frame is sufficient to evaluate perfusion due to the high extraction fraction of lipophilic radiotracers into the brain<sup>18,38,39</sup>. Nevertheless, not acquiring the full dynamic curve for 110 min is a limitation of this study. Further research is needed to validate our results with those derived from full dynamic analyses, which would provide a more comprehensive assessment of the potential bias introduced by our approach and help validate the reliability of our R1 estimates.

In this study, we used SUVR values obtained from 90 to 110 min as an indicator of amyloid burden. While SUVR is a widely used practical method to quantify amyloid deposition in clinical studies, it can be influenced by factors such as alterations in CBF or the rate of radiotracer clearance from the brain, potentially leading to biased estimates of  $A\beta$  burden. This influence of CBF on SUVR has been reported for  $^{11}\text{C}$ -Pittsburgh compound B (PiB) and  $^{18}\text{F}$ -florbetapir<sup>40,41</sup>. However, Bullich et al. reported that late time point SUVR also provided accurate results, with a limited impact of CBF and excellent correlation with full tracer kinetics on  $^{18}\text{F}$ -florbetaben PET scans<sup>36</sup>. They found that SUVR acquired from 120 to 140 min showed a stronger linear correlation with  $\text{BP}_{\text{ND}}$  derived from the 2-tissue compartment model using 0–140 min data compared to  $\text{BP}_{\text{ND}}$  obtained using SRTM and a 0–30/120–140 min dual-time window acquisition. On the other hand, Heeman et al. reported that the 0–30 min/90–110 min dual-time window protocol is the optimal approach for accurately estimating  $\text{BP}_{\text{ND}}$  values from  $^{18}\text{F}$ -florbetaben data, and that there is an increase in bias of amyloid estimates for larger intervals. This suggests that the  $\text{BP}_{\text{ND}}$  values obtainable from our 0–10 min/90–110 min protocol may also be biased. Therefore, further research is needed to compare  $\text{BP}_{\text{ND}}$  values obtained from the full dynamic curve with SUVR and  $\text{BP}_{\text{ND}}$  values derived from our dual-time window acquisition protocol.

Fazlollahi et al. revealed a positive correlation between CBF measured using ASL MRI and  $A\beta$  burden measured with  $^{11}\text{C}$ -PiB PET, specifically in cognitively normal individuals with  $A\beta^+$  (preclinical AD)<sup>11</sup>. In their study, a significant correlation was not observed between  $A\beta$  and CBF in the general cognitively normal population. This could be attributed to the constrained variability in amyloid levels among individuals. This is especially those within the cognitively normal  $A\beta^-$  group. However, in our study, despite the similarly restricted range of amyloid levels in the  $A\beta^-$  CN group, we observed a significant correlation between amyloid and CBF across the entire cognitively normal population. The scatter plot of global R1 and dFBB SUVR (Fig. 8A) suggests that the positive correlation between global SUVR and R1 is primarily driven by subjects with higher amyloid burden, with the most pronounced effect observed in the high amyloid group. To better characterize this relationship, we conducted subgroup analyses comparing R1 values among low (Centiloid < 20), intermediate (Centiloid 20–40), and high (Centiloid > 40) amyloid burden groups. The results revealed a gradual increase in R1 values with increasing amyloid burden (Supplemental Fig. 5). Post-hoc analyses showed a significant R1 increase in the intermediate group compared to the low group, but no statistically significant difference between the

intermediate and high groups. These findings suggest that the hyperperfusion effect may be more prominent in the early stages of amyloid accumulation (intermediate group), with limited further increases at higher levels of amyloid burden (high group). An alternative hypothesis is that as amyloid pathology progresses, other factors (e.g., damage caused by neurotoxicity or inflammatory responses) may interact with the mechanisms driving hyperperfusion, potentially attenuating the magnitude of R1 increase in the high amyloid group. However, the small sample size in the high amyloid group ( $n=9$ ) may have limited the statistical power to detect significant changes in R1 from the intermediate to high groups. Therefore, these results should be interpreted with caution. To further investigate this relationship, future studies should include a larger sample of cognitively unimpaired subjects with high amyloid burden.

In conclusion, our study demonstrates that increased amyloid burden is associated with higher relative perfusion, as measured by the R1 parameter derived from the early phase of dynamic amyloid PET scans, in cognitively normal individuals. The positive correlation between R1 and amyloid burden may indicate a compensatory mechanism in the preclinical stage of Alzheimer's disease. To further elucidate the complex interplay between CBF and amyloid accumulation in the asymptomatic stage, longitudinal observational studies monitoring A $\beta$  and CBF changes in cognitively normal individuals with A $\beta$ -negativity but at high risk of AD are needed. Our clinically feasible dual-phase PET protocol allows for the simultaneous assessment of amyloid burden and neuronal dysfunction, facilitating a direct comparison between these biomarkers within the same patient and time point. While the lack of full dynamic scans is a limitation, previous research suggests that the early time frame is sufficient for evaluating perfusion. Nevertheless, further studies are needed to validate our findings against full dynamic analyses.

## Materials and methods

### Study population

This study adhered to the principles outlined in the 1975 Declaration of Helsinki (2013 revision). All participants provided written informed consent. The Institutional Review Board of Ewha Womans University Mokdong Hospital approved the study (IRB approval number: 2020-11-004). Between June 2020 and February 2023, we included 71 normal older adults ( $\geq 60$  years old) demonstrating normal cognitive function and completing dual-phase  $^{18}\text{F}$ -FBB scanning. Normal cognitive function was defined as scores of 26 or higher on the Korean Mini-Mental State Examination, 2nd edition (K-MMSE 2), and a Global Clinical Dementia Rating (CDR) of 0, along with neuropsychological test scores within the normative range ( $-1.5$  standard deviations or higher) adjusted for the individual's age, sex, and educational background. Individuals with any of the following features were excluded: (1) suspected or diagnosed with dementia or mild cognitive impairment; (2) suspected or diagnosed with major neurological or psychiatric conditions, such as major depressive disorders; (3) a history of medications known to affect cognitive and emotional functions within the last 3 months; or (4) any other significant medical conditions. Each participant underwent a comprehensive assessment, including routine clinical assessment, neurological examinations, laboratory and neuropsychological tests, and neuroimaging studies such as MRI.

A $\beta$  negativity and A $\beta$  positivity were determined based on the standardized uptake value ratio (SUVR) as well as the Centiloid scale obtained from amyloid PET scans. Participants with an SUVR  $< 1.08$  (Centiloid  $< 20$ ) were classified as belonging to the A $\beta$ -negative cognitively normal (A $\beta$ -NC) group, while those with a value  $> 1.08$  (Centiloid  $> 20$ ) were classified as belonging to the A $\beta$ -positive cognitively normal (A $\beta$ +NC) group, following criteria established in a previous study<sup>42,43</sup>.

### $^{18}\text{F}$ -FBB PET imaging

All  $^{18}\text{F}$ -FBB PET/CT processes were performed following our established institutional guidelines. Dynamic PET images were taken using a dedicated PET/CT scanner (Biograph mCT, Siemens) in three-dimensional (3D) list mode. The early phase scan was performed immediately following a bolus injection of  $308.12 \pm 10.93$  MBq  $^{18}\text{F}$ -FBB, which lasted for 10 min (0–10 min after injection, eFBB). Subsequently, the delayed phase scan, lasting for 20 min (90–110 min post-injection, dFBB), was obtained. A spiral CT scan of the brain was obtained with CT parameters determined at 120 kV, 30 mAs, and a 1.0 mm slice thickness. The CT data were utilized to correct for attenuation in the PET emission data. To mitigate motion artifacts, the head of the participant was secured by employing a head holder and fixation equipment, including a vacuum cushion. The conventional PET data underwent reconstruction into a  $128 \times 128$  matrix (voxel size:  $3.18 \times 3.18 \times 2.02$  mm<sup>3</sup>) utilizing the built-in 3D ordered subset expectation maximization algorithm with four iterations, twelve subsets, and a 5-mm Gaussian filter. These data were then averaged into single frames for eFBB and dFBB. In addition, the 10-min list-mode data from the early-stage scan underwent reconstruction into 15 frames ( $6 \times 5$ ,  $3 \times 10$ ,  $4 \times 60$ , and  $2 \times 150$  s) to compute the SRTM-based R1. Parametric R1 maps at the voxel level were produced employing the SRTM method, implemented in PXM0D v4.0, with the cerebellum serving as the reference region, as previously described<sup>20,44</sup>.

### VOI-based analysis

As previously described<sup>20</sup>, registration of dual-phase  $^{18}\text{F}$ -FBB PET (0–10 min, 90–110 min) and R1 map-to-3D T1 MRI was conducted employing PM0D v4.0 (PM0D Technologies Ltd., Zurich, Switzerland). Volumes of interest (VOIs) were outlined employing an automated Maximum Probability Atlas technique (pmod.com/files/download/v35/doc/pneuro/5675.htm), incorporating three probability maps for MRI segmentation for each participant, along with the Automated Anatomical Labeling atlas. These VOIs covered cortical gray matter target areas (including frontal, posterior cingulate and precuneus [PCC/PC], lateral parietal, lateral temporal, medial temporal, and occipital cortices) and the reference area (whole cerebellum). The standardized uptake values (SUVs) of the different target regions were divided by the SUV of the reference region, yielding regional SUV ratios (SUVRs) for eFBB and dFBB. The global SUVR was defined as a volume-weight average of the

values from all target regions including frontal, PCC/PC, lateral parietal, lateral temporal, medial temporal, and occipital cortices.

### Voxel-based analysis

In addition to the VOI examination, a voxel-based analysis of eFBB, dFBB, and R1 maps were conducted utilizing Statistical Parametric Mapping software (SPM12; Wellcome Department of Cognitive Neurology, London, UK) integrated in MATLAB R2017a (MathWorks Inc., Natick, MA). The R1 maps of each participant were coregistered to their corresponding T1 MR images. For spatial standardization, the MR images of each participant underwent segmentation employing the tissue probability map in SPM12, following image-intensity nonuniformity correction. Nonlinear transformation parameters were then computed to align the original space images with the Montreal Neurological Institute space. The transformation matrix was employed on every R1 image, which had previously undergone coregistration with the T1 MR image. Subsequently, each R1 image underwent smoothing using an 8-mm full-width at half-maximum Gaussian kernel. A voxel-based two-sample *t*-test was performed to assess the differences in the distribution patterns of R1 images between the A $\beta$ <sup>-</sup>NC and A $\beta$ <sup>+</sup>NC groups. Statistical significance was established at  $p < 0.05$  with correction for false discovery rate (FDR) and an extent cluster threshold of  $> 100$  voxels.

### Neuropsychological assessments

Neuropsychological evaluations were performed employing the SNSB<sup>45</sup>. General cognition was evaluated using the K-MMSE 2 and CDR<sup>46,47</sup>. Specific tests within the SNSB encompassed the digit span (forward and backward) tests to evaluate attention, Korean version of the Boston Naming Test (K-BNT) for language evaluation, Rey–Osterrieth Complex Figure Test (RCFT) for visuospatial and memory function assessment, Seoul Verbal Learning Test (SVLT) for memory function evaluation, and Controlled Oral Word Association Test (COWAT) with Stroop color reading test for evaluating frontal/executive function. Standardized *Z*-scores, adjusted for age, sex, and education, were utilized for result analysis.

### Statistical analyses

All statistical analyses were conducted utilizing two commercial software programs: IBM SPSS Statistics (version 26.0, Armonk, NY, USA) and Rex 3.6.0 (Rexsoft, Seoul, Korea). Differences in demographics and cognitive profiles between the two groups were examined using Fisher's exact test for categorical variables, while the Student's *t*-test was employed for continuous variables. Student's *t*-tests were also used to explore differences in SUVR and R1 values in global and target regions between both groups.

Pearson correlation analysis was employed to assess the relationships between SUVR and R1 values. As a partial correlation analysis, age, gender, years of education, and CDR scores were adjusted to evaluate the relationship between SUVR and R1 values, while age, gender, and years of education were adjusted to evaluate the relationship between global values and cognitive scores. A  $p < 0.05$  was deemed statistically significant.

### Data availability

The datasets generated or analyzed during the study can be obtained from the corresponding author upon reasonable request.

Received: 11 March 2024; Accepted: 30 July 2024

Published online: 09 August 2024

### References

- Association, A. 2018 Alzheimer's disease facts and figures. *Alzheimers Dement.* **14**, 367–429 (2018).
- Jack, C. R. *et al.* Hypothetical model of dynamic biomarkers of the Alzheimer's pathological cascade. *Lancet Neurol.* **9**, 119–128 (2010).
- Salloway, S. *et al.* Two phase 3 trials of bapineuzumab in mild-to-moderate Alzheimer's disease. *N. Engl. J. Med.* **370**, 322–333 (2014).
- Slomski, A. A $\beta$ -clearing drug fails to slow alzheimer disease. *Jama* **319**, 2470–2470 (2018).
- Sperling, R. A. *et al.* Toward defining the preclinical stages of Alzheimer's disease: Recommendations from the National Institute on Aging–Alzheimer's Association workgroups on diagnostic guidelines for Alzheimer's disease. *Alzheimer's Dement.* **7**, 280–292 (2011).
- Jagust, W. J. *et al.* Relationships between biomarkers in aging and dementia. *Neurology* **73**, 1193–1199 (2009).
- Johnson, S. C. *et al.* Amyloid burden and neural function in people at risk for Alzheimer's Disease. *Neurobiol. Aging* **35**, 576–584 (2014).
- Knopman, D. S. *et al.* Selective worsening of brain injury biomarker abnormalities in cognitively normal elderly persons with  $\beta$ -amyloidosis. *JAMA Neurol.* **70**, 1030–1038 (2013).
- Oh, H., Habeck, C., Madison, C. & Jagust, W. Covarying alterations in A $\beta$  deposition, glucose metabolism, and gray matter volume in cognitively normal elderly. *Hum. Brain Mapp.* **35**, 297–308 (2014).
- Sojkova, J. *et al.* Longitudinal cerebral blood flow and amyloid deposition: An emerging pattern?. *J. Nucl. Med.* **49**, 1465–1471 (2008).
- Fazlollahi, A. *et al.* Increased cerebral blood flow with increased amyloid burden in the preclinical phase of alzheimer's disease. *J. Magn. Reson. Imaging* **51**, 505–513 (2020).
- Michels, L. *et al.* Arterial spin labeling imaging reveals widespread and A $\beta$ -independent reductions in cerebral blood flow in elderly apolipoprotein epsilon-4 carriers. *J. Cereb. Blood Flow Metab.* **36**, 581–595 (2016).
- Jack, C. R. *et al.* Tracking pathophysiological processes in Alzheimer's disease: An updated hypothetical model of dynamic biomarkers. *Lancet Neurol.* **12**, 207–216 (2013).
- Riederer, I. *et al.* Alzheimer disease and mild cognitive impairment: Integrated pulsed arterial spin-labeling MRI and <sup>18</sup>F-FDG PET. *Radiology* **288**, 198–206 (2018).

15. Korte, N., Nortley, R. & Attwell, D. Cerebral blood flow decrease as an early pathological mechanism in Alzheimer's disease. *Acta Neuropathol.* **140**, 793–810 (2020).
16. Zlokovic, B. V. Neurovascular pathways to neurodegeneration in Alzheimer's disease and other disorders. *Nat. Rev. Neurosci.* **12**, 723–738 (2011).
17. Padrela, B. E. *et al.* Genetic, vascular and amyloid components of cerebral blood flow in a preclinical population. *J. Cereb. Blood Flow Metab.* **43**, 1726–1736 (2023).
18. Ottoy, J. *et al.* <sup>18</sup>F-FDG PET, the early phases and the delivery rate of <sup>18</sup>F-AV45 PET as proxies of cerebral blood flow in Alzheimer's disease: Validation against <sup>15</sup>O-H<sub>2</sub>O PET. *Alzheimer's & Dement.* **15**, 1172–1182 (2019).
19. Peretti, D. E. *et al.* Relative cerebral flow from dynamic PIB scans as an alternative for FDG scans in Alzheimer's disease PET studies. *PLoS One* **14**, e0211000 (2019).
20. Yoon, H.-J. *et al.* Dual-phase <sup>18</sup>F-florbetaben PET provides cerebral perfusion proxy along with beta-amyloid burden in Alzheimer's disease. *NeuroImage Clin.* **31**, 102773 (2021).
21. Lopes Alves, I. *et al.* Quantitative amyloid PET in Alzheimer's disease: The AMYPAD prognostic and natural history study. *Alzheimer's & Dement.* **16**, 750–758 (2020).
22. Thomas, T., Thomas, G., McLendon, C., Sutton, T. & Mullan, M.  $\beta$ -Amyloid-mediated vasoactivity and vascular endothelial damage. *Nature* **380**, 168–171 (1996).
23. Iadecola, C. *et al.* SOD1 rescues cerebral endothelial dysfunction in mice overexpressing amyloid precursor protein. *Nat. Neurosci.* **2**, 157–161 (1999).
24. Niwa, K. *et al.* A $\beta$ 1–40-related reduction in functional hyperemia in mouse neocortex during somatosensory activation. *Proc. Natl. Acad. Sci.* **97**, 9735–9740 (2000).
25. Bell, R. D. *et al.* SRF and myocardin regulate LRP-mediated amyloid- $\beta$  clearance in brain vascular cells. *Nat. Cell Biol.* **11**, 143–153 (2009).
26. Chow, N. *et al.* Serum response factor and myocardin mediate arterial hypercontractility and cerebral blood flow dysregulation in Alzheimer's phenotype. *Proc. Natl. Acad. Sci.* **104**, 823–828 (2007).
27. Ferrando, R. & Damian, A. Brain SPECT as a biomarker of neurodegeneration in dementia in the era of molecular imaging: Still a valid option?. *Front. Neurol.* **12**, 629442 (2021).
28. Leijenaar, J. F. *et al.* Lower cerebral blood flow in subjects with Alzheimer's dementia, mild cognitive impairment, and subjective cognitive decline using two-dimensional phase-contrast magnetic resonance imaging. *Alzheimer's Dement. Diagn. Assess. Dis. Monit.* **9**, 76–83 (2017).
29. Dai, W. *et al.* Mild cognitive impairment and Alzheimer disease: Patterns of altered cerebral blood flow at MR imaging. *Radiology* **250**, 856–866 (2009).
30. Zlatar, Z. Z., Wierenga, C. E., Bangen, K. J., Liu, T. T. & Jak, A. J. Increased hippocampal blood flow in sedentary older adults at genetic risk for Alzheimer's disease. *J. Alzheimer's Dis.* **41**, 809–817 (2014).
31. Bangen, K. J. *et al.* Assessment of Alzheimer's disease risk with functional magnetic resonance imaging: An arterial spin labeling study. *J. Alzheimer's Dis.* **31**, S59–S74 (2012).
32. Sperling, R. A. *et al.* Amyloid deposition is associated with impaired default network function in older persons without dementia. *Neuron* **63**, 178–188 (2009).
33. Mormino, E. C. *et al.* A $\beta$  deposition in aging is associated with increases in brain activation during successful memory encoding. *Cereb. Cortex* **22**, 1813–1823 (2012).
34. Binnewijzend, M. A. *et al.* Cerebral perfusion in the prodementia stages of Alzheimer's disease. *Eur. Radiol.* **26**, 506–514 (2016).
35. Tiepolt, S. *et al.* Early [<sup>18</sup>F] florbetaben and [<sup>11</sup>C] PiB PET images are a surrogate biomarker of neuronal injury in Alzheimer's disease. *Eur. J. Nucl. Med. Mol. Imaging* **43**, 1700–1709 (2016).
36. Bullich, S. *et al.* Validation of noninvasive tracer kinetic analysis of <sup>18</sup>F-florbetaben PET using a dual-time-window acquisition protocol. *J. Nucl. Med.* **59**, 1104–1110 (2018).
37. Heeman, F. *et al.* Optimized dual-time-window protocols for quantitative [<sup>18</sup>F] flutemetamol and [<sup>18</sup>F] florbetaben PET studies. *EJNMMI Res.* **9**, 1–14 (2019).
38. Forsberg, A., Engler, H., Blomquist, G., Långström, B. & Nordberg, A. The use of PIB-PET as a dual pathological and functional biomarker in AD. *Biochim. Biophys. Acta (BBA)-Mol. Basis Dis.* **1822**, 380–385 (2012).
39. Lin, K.-J. *et al.* Imaging characteristic of dual-phase <sup>18</sup>F-florbetapir (AV-45/Amyvid) PET for the concomitant detection of perfusion deficits and beta-amyloid deposition in Alzheimer's disease and mild cognitive impairment. *Eur. J. Nucl. Med. Mol. Imaging* **43**, 1304–1314 (2016).
40. van Berckel, B. N. *et al.* Longitudinal amyloid imaging using <sup>11</sup>C-PiB: Methodologic considerations. *J. Nucl. Med.* **54**, 1570–1576 (2013).
41. Ottoy, J. *et al.* Validation of the semiquantitative static SUVR method for <sup>18</sup>F-AV45 PET by pharmacokinetic modeling with an arterial input function. *J. Nucl. Med.* **58**, 1483–1489 (2017).
42. Royse, S. K. *et al.* Validation of amyloid PET positivity thresholds in centiloids: A multisite PET study approach. *Alzheimer's Res. Ther.* **13**, 99 (2021).
43. Rafii, M. S. *et al.* The AHEAD 3–45 study: Design of a prevention trial for Alzheimer's disease. *Alzheimer's Dement.* **19**, 1227–1233 (2023).
44. Meyer, P. T. *et al.* Dual-biomarker imaging of regional cerebral amyloid load and neuronal activity in dementia with PET and <sup>11</sup>C-labeled Pittsburgh compound B. *J. Nucl. Med.* **52**, 393–400 (2011).
45. Ryu, H. J. & Yang, D. W. The Seoul neuropsychological screening battery (SNSB) for comprehensive neuropsychological assessment. *Dement. Neurocogn. Disord.* **22**, 1 (2023).
46. Baek, M. J., Kim, K., Park, Y. H. & Kim, S. The validity and reliability of the mini-mental state examination-2 for detecting mild cognitive impairment and Alzheimer's disease in a Korean population. *PLoS One* **11**, e0163792 (2016).
47. Choi, S.-H. *et al.* Estimating the validity of the Korean version of expanded clinical dementia rating (CDR) scale. *J. Korean Neurol. Assoc.* **585–591** (2001).

## Acknowledgements

This research was supported by the Korea Health Technology R&D Project through the Korea Health Industry Development Institute (KHIDI), funded by the Ministry of Health & Welfare and Ministry of Science and ICT, Republic of Korea (grant number: HU20C0271). Additionally, it was funded by the National Research Foundation of South Korea (grant number: NRF-2021R1A2C1093636).

## Author contributions

Conceptualization: Geon Ha Kim, Hai-Jeon Yoon, and Jee Hyang Jeong. Data curation: Geon Ha Kim, Bori R. Kim, and Hai-Jeon Yoon. Formal analysis: Geon Ha Kim, Hai-Jeon Yoon, and Jee Hyang Jeong. Funding acquisition: Geon Ha Kim, Hai-Jeon Yoon, and Jee Hyang Jeong. Investigation: Geon Ha Kim, Hai-Jeon Yoon, and Jee Hyang Jeong. Methodology: Geon Ha Kim and Bori R. Kim. Project administration: Geon Ha Kim, Hai-Jeon

Yoon, and Jee Hyang Jeong. Resources: Geon Ha Kim, Hai-Jeon Yoon, and Jee Hyang Jeong. Software: Hai-Jeon Yoon. Supervision: Hai-Jeon Yoon and Jee Hyang Jeong. Validation: Geon Ha Kim, Bori R. Kim, Hai-Jeon Yoon, and Jee Hyang Jeong. Visualization: Bori R. Kim and Hai-Jeon Yoon. Writing-original draft: Geon Ha Kim and Hai-Jeon Yoon. Writing-review & editing: All

### Competing interests

The authors declare no competing interests.

### Additional information

**Supplementary Information** The online version contains supplementary material available at <https://doi.org/10.1038/s41598-024-68916-4>.

**Correspondence** and requests for materials should be addressed to H.-J.Y. or J.H.J.

**Reprints and permissions information** is available at [www.nature.com/reprints](http://www.nature.com/reprints).

**Publisher's note** Springer Nature remains neutral with regard to jurisdictional claims in published maps and institutional affiliations.



**Open Access** This article is licensed under a Creative Commons Attribution-NonCommercial-NoDerivatives 4.0 International License, which permits any non-commercial use, sharing, distribution and reproduction in any medium or format, as long as you give appropriate credit to the original author(s) and the source, provide a link to the Creative Commons licence, and indicate if you modified the licensed material. You do not have permission under this licence to share adapted material derived from this article or parts of it. The images or other third party material in this article are included in the article's Creative Commons licence, unless indicated otherwise in a credit line to the material. If material is not included in the article's Creative Commons licence and your intended use is not permitted by statutory regulation or exceeds the permitted use, you will need to obtain permission directly from the copyright holder. To view a copy of this licence, visit <http://creativecommons.org/licenses/by-nc-nd/4.0/>.

© The Author(s) 2024